JOURNAL OF CATALYSIS 92, 119–126 (1985)

A Study of the Catalytically Active Copper Species in the Synthesis of Methanol Over Cu–Cr Oxide

J. R. MONNIER, M. J. HANRAHAN, AND G. APAI

Research Laboratories, Eastman Kodak Company, Rochester, New York 14650

Received March 6, 1984; revised November 1, 1984

Cu–Cr oxide catalysts formulated with various Cu/Cr ratios were prepared and evaluated as CH_3OH synthesis catalysts. From the physical characterization of these catalysts by X-ray diffraction, X-ray photoelectron spectroscopy, and temperature-programmed desorption of CO, Cu^+ was identified as the active site responsible for CO chemisorption and CH_3OH formation. The Cu^+ is stable under reaction conditions and exists as a crystalline $CuCrO_2$ phase. The concentration of surface Cu^+ (or $CuCrO_2$) is dependent upon the Cu/Cr ratio, the calcination temperature, and the nature of the catalyst pretreatment.

INTRODUCTION

Copper–chromium oxide is a selective methanol synthesis catalyst (*1, 2*) and shares features common to the Cu–ZnO methanol synthesis catalyst, which has been discussed in considerable detail by Herman *et al.* (*3, 4*). For both catalysts, the active sites for associative CO adsorption and subsequent CH_3OH formation are reported to be Cu^+ ions. In the Cu–ZnO system, Herman (*3*), using optical absorption spectroscopy, deduced that the Cu^+ ions are positioned substitutionally and/or interstitially in the ZnO lattice. The ZnO lattice provided the hydrogenation sites for the adsorbed CO. Recently, Apai *et al.* (*5*), using X-ray photoelectron spectroscopy, have shown a direct correlation between surface Cu^+ ions and the rate of CH_3OH formation over Cu–Cr oxide. However, for Cu–Cr oxide little is known about the environment of the Cu^+ site responsible for CO adsorption and activation.

We present here the effects of catalyst composition and preparation on the catalytic activities for CH_3OH formation and surface properties of Cu–Cr oxide. Specifically, correlations between the amount of surface Cu^+ and CH_3OH activity are presented; in addition, the Cu^+-containing surface phase is identified. The nature of the hydrogenation sites in Cu–Cr oxide will be the subject of another paper.

EXPERIMENTAL

Catalyst Preparation

All catalysts were prepared by the decomposition of homogeneous citrate complexes by methods similar to those described by Courty *et al.* (*6*). Briefly, citric acid was added to an aqueous solution (all at 300 K) of the appropriate molar quantities of Cu^{2+} and Cr^{3+} acetates to form the corresponding Cu^{2+}–Cr^{3+} citrate complex. For the formation of Cr_2O_3 and CuO, citric acid was added to aqueous solutions of Cr^{3+} acetate and Cu^{2+} acetate, respectively. The resulting slurry was evaporated to dryness on a steam bath to form a translucent solid, which was dried at 150°C in a flowing N_2 stream for 2 h. The dry solid was ground to a powder for calcination and catalyst pretreatment.

Because the calcination was highly exothermic above 200°C, the calcination temperature was continuously monitored by means of a sheathed thermocouple imbedded within the catalyst sample. During the initial stages of the calcination, the temper-

0021-9517/85 $3.00

ature was kept below 350°C by varying the percentage of O_2 in the He stream. Typically, 4–8% O_2 was required to keep the catalyst from exotherming. Only during the latter stages of calcination could the O_2 level be increased to the normal 20%. All catalysts were given final calcinations for 2 h between 300 and 400°C in 20% O_2/80% He. Unregulated use of O_2 during initial stages of calcination often produced temperature excursions in excess of 600°C.

Before kinetic evaluation, all catalysts were reduced/pretreated at 270°C in flowing H_2 at 1 atm pressure for 1–2 h. This process was also exothermic above 160°C during the initial stages of the H_2 pretreatment. The exothermicity was more pronounced for the catalysts with high Cu/Cr ratios and was linked to the amount of H_2O produced during the reduction. After the initial surge of H_2O formation, exothermicity ceased and the pretreatment/reduction process was thermally stable. If unregulated, however, the temperature during the initial stages of catalyst pretreatment could go over 400°C. The temperature was regulated by externally cooling the catalyst in a stream of flowing N_2.

Catalyst Evaluation

All catalysts were evaluated in a single-pass, high-pressure flow reactor. High-pressure reaction conditions were maintained by using a back-pressure regulator downstream from the reactor and upstream from the in-line gas-sampling loop used for gas chromatographic (GC) analysis. All lines below the reactor were kept above 100°C to prevent product condensation. To minimize catalytic wall reactions in the stainless-steel tube reactor, the inside walls of the tube were gold plated. Reaction conditions (unless otherwise specified) were 270°C, feed composition of $H_2/CO = 2/1$, and overall pressure of 900 psig. In all cases, CO conversion was kept at less than 2%. To remove trace amounts of $Fe(CO)_5$ from the CO feed stream, a molecular-sieve 5A trap kept at 200°C was inserted in the feed manifold upstream from the catalyst.

Catalyst Characterization

A. Elemental analyses. The Cu and Cr weight percentages were determined by neutron activation analysis, and that of O was taken to be the remainder of the total weight. For most catalysts, elemental analyses were obtained after calcination at 350°C and after H_2 reduction at 270°C to gain some estimate of the amount of lattice oxygen lost during reduction.

B. X-Ray diffraction. Powder X-ray diffraction patterns were obtained over the 2θ interval of 4–60° with a Siemens type F diffractometer using Cu$K\alpha$ ($\lambda = 1.5418$ Å) irradiation. For some specific catalysts, X-ray diffraction analyses were made after calcination and after reduction to determine whether the oxygen loss during reduction gave rise to any new bulk crystalline phases.

C. Surface area determination. Surface areas were obtained with a Micrometrics Digisorb 2500 multisample surface area analyzer. All surface areas were derived from multipoint BET adsorption isotherms, with N_2 at −195°C as the adsorbate. For some catalysts, surface areas were measured after calcination and after H_2 reduction to determine the effect of reduction on surface area.

D. X-Ray photoelectron spectroscopy (XPS). Samples undergoing pretreatments identical to those used for the catalysts being evaluated at reaction conditions were mounted on a resistively heated boat and reduced for 1 h at 270°C in a preparation chamber attached to an ultrahigh-vacuum XPS analysis chamber. XPS data were obtained by using unmonochromatized Mg$K\alpha$ radiation ($h\nu = 1253.6$ eV) and an analyzer resolution of 0.4 eV. Binding energies of photoemission and Auger peaks were determined by assigning the carbon 1*s* peak of the adventitious carbon to have a binding energy of 284.6 eV. Since our studies focused mainly on the oxidation states of cop-

TABLE 1

Composition of Cu–Cr Oxide Catalysts after Calcination at 350°C and after H_2 Reduction at 295°C

Catalyst	Calcined catalyst		Reduced catalyst		Oxygen lost[a] (%)
	Empirical formula	Surface area (m^2/g)	Empirical formula	Surface area (m^2/g)	
100% CuO	CuO	—	Cu^0	<5	100
9/1 Cu–Cr oxide	$Cu_8Cr_1O_{9.5}$	33.0	$Cu_8Cr_1O_{2.4}$	19	75
2/1 Cu–Cr oxide	$Cu_2Cr_1O_{4.4}$	22.3	$Cu_2Cr_1O_{2.0}$	27.4	55
1/1 Cu–Cr oxide	$Cu_1Cr_{1.2}O_{3.8}$	—	$Cu_1Cr_{1.2}O_{2.5}$	53	34
1/2 Cu–Cr oxide	$Cu_1Cr_{1.8}$	66.4	—	78	—
1/4 Cu–Cr oxide	$Cu_1Cr_4O_{12}$	48.2	$Cu_1Cr_4O_{8.4}$	73	30
1/10 Cu–Cr oxide	$Cu_1Cr_{10}O_{26}$	34.7	$Cu_1Cr_{10}O_{15}$	34.2	7
1/50 Cu–Cr oxide	$Cu_1Cr_{50}O_{94}$	40.9	$Cu_1Cr_{50}O_{86}$	39.8	9
100% Cr_2O_3	$Cr_2O_{3.3}$	70.6	Cr_2O_3	64.4	9

[a] The percentage of oxygen lost during reduction is calculated from differences in the empirical formulae for a given catalyst.

per using the Auger parameters, the possible problems associated with charge referencing were not experienced.

E. Temperature-programmed desorption (TPD) of CO. The TPD technique was a dynamic one in which He at 80 (STP) ml/min was used as a sweep gas to transfer the desorbed gases from the Cu–Cr oxide surface to the differentially pumped inlet system of a UTI Model Q-30C quadrupole mass spectrometer. Before the TPD spectrum was run, CO was chemisorbed onto the H_2-reduced and vacuum-pretreated Cu–Cr oxide surface at 25°C from a flowing stream of CO. Reversibly adsorbed CO was removed from the surface by evacuating to 10^{-2} Torr before the TPD experiment was conducted. During the desorption experiment, selected mass intensities and the catalyst temperature were stored on a UTI Model 2054 programmable peak selector directly interfaced with the Q-30C mass spectrometer. The linear temperature ramp was maintained by a Theall Model TP-2200 temperature programmer.

RESULTS AND DISCUSSION

The compositions of the catalysts are shown in Table 1 for the calcined and reduced states. The physical properties of the H_2-reduced catalysts should more closely resemble the properties of the catalysts under H_2/CO reaction conditions. Several points are apparent from examination of Table 1. First, the Cu/Cr ratios of the analyzed samples are quite close to the nominal ratios, as one would expect for a coprecipitation type of preparation. Second, the surface areas of the catalysts decrease as the amount of Cu in the catalysts increases (20–100% Cu levels); in addition, H_2 reduction has a minimal effect on the surface areas of the catalysts. Finally, the amount of lattice oxygen lost during H_2 reduction increases dramatically as the composition changes from 100% Cr_2O_3 to 100% CuO, indicating the reduction of CuO to metallic Cu^0 upon exposure to H_2 at 300°C.

The X-ray diffraction data summarized in Table 2 support the oxygen loss trend in Table 1 and indicate that reduction of CuO to Cu^0 occurs upon exposure to H_2 at 270°C. These X-ray data agree with the data of Schreifels *et al.* (*7*), who observed that most of the Cu in calcined Cu–Cr oxide catalysts exists as CuO. Likewise, on the basis of XPS, Capece and co-workers (*8*) and Apai *et al.* (*5*) have stated that, upon reduction, the CuO in Cu–Cr_2O_3 catalysts is reduced to Cu^0.

TABLE 2

X-Ray Diffraction Summary for Cu–Cr Oxide Catalysts; Identified Crystalline Components Presented as a Function of Their Relative Concentrations[a]

Catalyst	Calcined	Reduced
9/1 Cu–Cr oxide	CuO (Only)	Cu^0 (Major) $CuCrO_2$ (Minor) $CuCr_2O_4$ (Trace)
2/1 Cu–Cr oxide	CuO (Major) Cr_2O_3 (Minor) $CuCr_2O_4$ (Small)	Cu^0 (Major) $CuCrO_2$ (Minor) $CuCr_2O_4$ (Small)
1/1 Cu–Cr oxide	CuO, Cr_2O_3 (Major) $CuCr_2O_4$ (Small)	Cu^0 (Major) $CuCr_2O_4$ (Minor) $CuCrO_2$ (Minor)[b]
1/2 Cu–Cr oxide	Cr_2O_3 (Major) CuO (Minor) $CuCr_2O_4$ (Trace)	(Not done)
1/4 Cu–Cr oxide	Cr_2O_3 (Major) CuO (Small)	(Not done)
1/10 Cu–Cr oxide	Cr_2O_3 (Only)	Cr_2O_3 (Major) Cu^0 (Trace)
100% Cr_2O_3	Cr_2O_3 (Only)	(Not done)

[a] Order of decreasing concentration: major > minor > small > trace.

[b] $CuCrO_2$ present as 50–100 Å crystallites, from X-ray line broadening.

The X-ray data of Table 2 reveal the existence of the spinel $CuCr_2O_4$ for the calcined forms of the catalysts with Cu/Cr ratios $\geq 1/2$. After reduction, X-ray diffraction also shows the existence of $CuCrO_2$. It is not possible to state from this study whether the $CuCrO_2$ is formed from the reduction of $CuCr_2O_4$ or is formed independently of $CuCr_2O_4$, since the X-ray diffraction peaks of CuO in the calcined form of the catalysts give essentially 100% interference with the principal diffraction lines of $CuCrO_2$. Only after the removal of the CuO diffraction peaks by reduction of CuO to Cu^0 is it possible to observe the diffraction pattern of $CuCrO_2$. Nevertheless, as stated above, the reduced forms of the Cu–Cr oxide catalysts are more likely to resemble the working catalyst under H_2/CO reaction conditions. Finally, the absence of any Cr_2O_3 diffraction lines after H_2 reduction of the 1/1 and 2/1 Cu–Cr oxide samples may be due to the formation of amorphous and/or small crystallites of Cr_2O_3 during the reduction, as discussed by Iimura *et al.* (*9*).

The specific activities for CH_3OH formation as a function of mole fraction Cu are plotted in Fig. 1. All catalytic activities were obtained at the steady state after a minimum of 4 h on stream. During the time on stream, only slight deactivation to the steady state was observed for all the catalysts, showing that the pretreatment in flowing H_2 had stabilized the active surface. Included in Fig. 1 is the integrated X-ray diffraction peak area for the (200) reflection of $CuCrO_2$ at $2\theta = 36°$. The surface areas used to calculate the specific rates of CH_3OH formation are for the H_2-reduced samples. Both the specific CH_3OH activity and the concentration of $CuCrO_2$ pass through a maximum at the copper mole fraction ≈ 0.7, suggesting a correlation between catalytic activity and the amount of crystalline $CuCrO_2$.

The X-ray data in Table 2 also reveal that $CuCr_2O_4$ is observed along with $CuCrO_2$. To determine the possible role of $CuCr_2O_4$ in CH_3OH synthesis, we evaluated a series

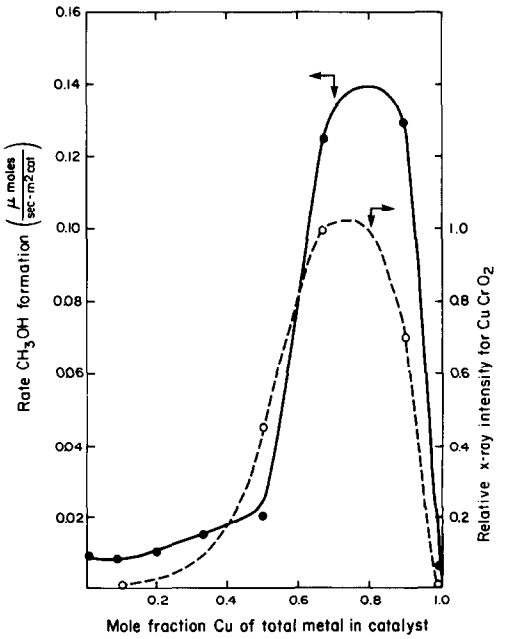

FIG. 1. Dependencies of specific CH_3OH activity and concentration of $CuCrO_2$ on the mole fraction of Cu in Cu–Cr oxide catalysts (●—●, CH_3OH formation rates; O---O, $CuCrO_2$ XRD intensity).

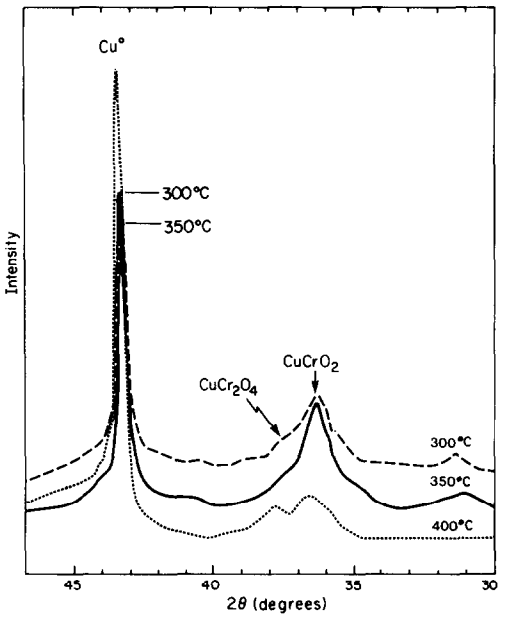

FIG. 2. X-Ray diffraction patterns and catalytic activities of 1/1 Cu–Cr oxides calcined at 300, 350, and 400°C. All catalysts were reduced at 270°C before X-ray diffraction analysis and catalytic evaluation.

of 1/1 Cu–Cr oxide catalysts, which were calcined at different temperatures (300, 350, and 400°C), for catalytic activity and examined them by X-ray diffraction. The results (summarized in Fig. 2 and Table 3) reveal that specific activity is highest for the sample calcined at 350°C. The X-ray diffraction data also show a maximum in $CuCrO_2$ peak intensity for the sample calcined at 350°C, whereas the $CuCr_2O_4$ peak intensity relative to the $CuCrO_2$ peak is highest for the sample calcined at 400°C. Since the catalytic activity at 400°C is lower than for the samples calcined at 300 and 350°C, it does not appear that catalytic activity is linked to the presence of $CuCr_2O_4$.

The data in Fig. 2 also suggest that there is an optimum calcination temperature (~350°C) for the Cu–Cr oxide catalysts. Temperatures <350°C result in incomplete formation of $CuCrO_2$ (or a $CuCrO_2$ precursor), whereas temperatures >350°C cause decomposition of $CuCrO_2$ (or its precursor), perhaps into $CuCr_2O_4$ and CuO. As the X-ray data in Table 2 indicated, CuO formed during calcination is totally reduced during H_2 reduction, explaining the large Cu^0 X-ray diffraction peak in Fig. 2 for the sample calcined at 400°C. These observations are in good agreement with those of Iimura and co-workers (*9*), who found that the CuO component of a Cu–Cr oxide catalyst was completely reduced to Cu^0 when the catalyst was pretreated in a recirculation reactor containing 50 Torr of H_2 at 200–300°C. Likewise, Iimura concluded that $CuCrO_2$ was stable to 400°C under the same reducing conditions.

We recorded X-ray photoelectron spectra for the 1/1 Cu–Cr oxide samples calcined at 300, 325, 350, 375, and 400°C and subsequently reduced in H_2 at 270°C to study the oxidation state(s) of the surface Cu species for these catalysts. These data are summarized in Fig. 3 and illustrate the fraction of surface Cu existing as Cu^+ as a function of calcination temperature. Cu^0 and Cu^+ contributions were determined from curves generated by adding together Cu(LMM) Auger spectra from copper metal and cuprous chromite in various ratios. Peak heights for each component were then measured above a linear background. Further details of the XPS results have been published (*5*). No Cu^{2+} species were detected in the Cu 2*p* core levels for the H_2-reduced samples, which eliminates the pos-

TABLE 3

Rate of CH_3OH Formation as a Function of Calcination Temperature for a 1/1 Cu–Cr Oxide Catalyst[a]

T_{calc} (°C)	$\left(\frac{\mu mole\ CH_3OH}{sec\text{-}m^2\ catalyst}\right)$
300	0.017
350	0.020
400	0.010
~500	0.007

[a] Uncertainty in rates is ±0.002.

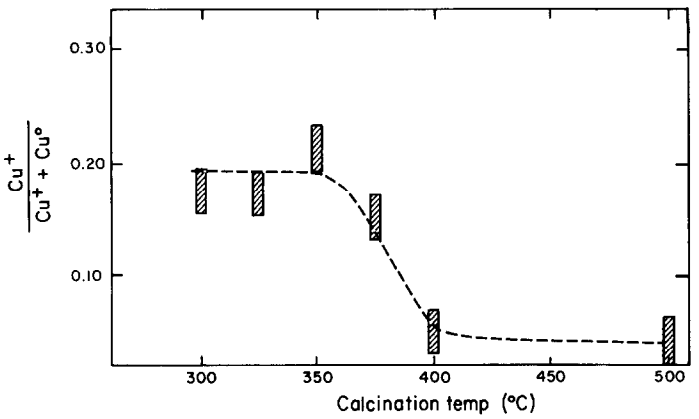

FIG. 3. Effect of calcination temperature on concentration of Cu^+ as determined by XPS. Catalyst is 1/1 Cu–Cr oxide. Each sample was reduced in H_2 at 270°C before analysis. Data for calcination temperatures of 325 and 375°C were obtained for a different catalyst and were thus normalized to a 350°C calcination temperature, which was common to both catalysts. The dashed line is intended to indicate trends only.

sibility that species such as CuO or Cu Cr_2O_4 are present at the surface. We find that the surface coverage of Cu^+ is largest for calcination temperatures between 300 and 350°C. The amount of Cu^+ vs Cu^0 sharply decreases at calcination temperatures >350°C. In general, this trend agrees with the X-ray diffraction curves of the bulk catalyst shown in Fig. 2. Comparison of Fig. 3 and Table 3 shows that there is a correlation between changes in catalytic activity and the surface concentration of Cu^+, which presumably exists within a stable, crystalline $CuCrO_2$ surface phase. Although we have observed variations of ~20% in the ratio of Cu^+ to total Cu for different sample batches yielding identical catalytic activity, the variations of that ratio with calcination temperature remain similar to those shown in Fig. 3.

Temperature-programmed desorption of CO from the 1/1 Cu–Cr oxide catalyst (calcined at 350°C) was used to determine the number of different types of CO adsorption sites and the strength of the CO binding energy. The TPD spectrum for this catalyst (Fig. 4) shows only one type of CO adsorption site. Burwell and co-workers (*10*) studied the chemisorption properties of Cr_2O_3 and found that only small amounts of CO were weakly adsorbed on Cr_2O_3; CO desorbed near room temperature. Thus, we can discount the possibility of CO chemisorption on Cr_2O_3 portions of the catalyst, since the X-ray data in Table 2 revealed that Cr_2O_3 was present in the 1/1 Cu–Cr oxide. Since XPS indicated that the only Cu species present were Cu^0 and Cu^+, and Pasquali *et al.* (*11*) have shown that Cu^0 does not chemisorb CO, we can conclude that the TPD curve represents desorption of CO from Cu^+ sites. Application of the Redhead equation for first-order desorption (*12*) of CO yields an apparent desorption energy of 26.4 kcal/mole. This relatively mild interaction between CO and Cu^+ is consistent with the reduction of associatively adsorbed CO to selectively form CH_3OH under H_2/CO reaction conditions. A stronger CO–surface interaction would be expected to give dissociatively adsorbed CO and subsequent hydrocarbon formation under H_2/CO reaction conditions (*13*).

To confirm the link between Cu^+ in $CuCrO_2$) and catalytic activity, we conducted an additional experiment. Stroupe (*14*) has shown that it is possible to selectively prepare $CuCrO_2$ from a typical Cu–

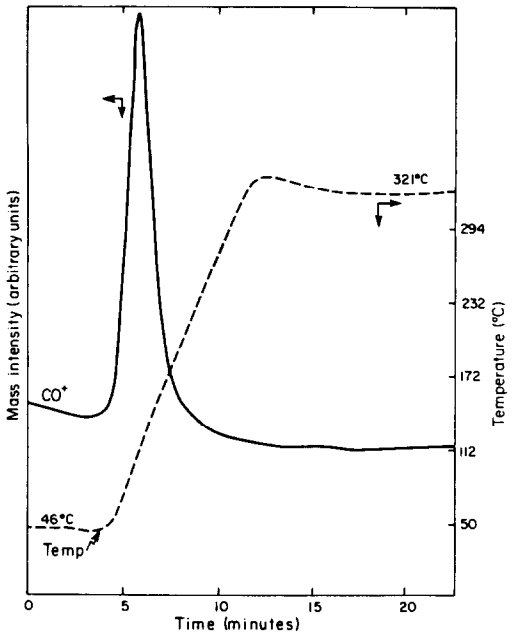

FIG. 4. TPD spectrum of CO for 1/1 Cu–Cr oxide calcined at 350°C. Desorption peak maximum at 134°C; heating rate 40°C/min.

Cr oxide catalyst (one calcined at 350°C) by using a high-temperature treatment. Briefly, the preparation involves the heat treatment of a normal Cu–Cr oxide catalyst in air at 600°C for 4–8 h to form $CuCr_2O_4$, followed by a second heat treatment at 900–1000°C for 24 h to form $CuCrO_2$. This preparation can be summarized as

$$\underset{\text{(1/1 Cu–Cr oxide)}}{2CuO \cdot Cr_2O_3} \xrightarrow[8\text{ h}]{600^\circ C} CuCr_2O_4$$

$$+ CuO \xrightarrow[24\text{ h}]{900^\circ C} 2CuCrO_2 + \tfrac{1}{2}O_2$$

The characterization and CH_3OH activity determined from a catalyst prepared in this way are summarized in Table 4. As a result of the high-temperature treatment, more $CuCrO_2$ was formed and the fraction of surface Cu^+ was substantially higher than for the sample calcined at 350°C. The specific rate for CH_3OH formation was also proportionally higher for the sample calcined at 1000°C, providing even further correlation between catalytic activity and surface concentration of stable Cu^+, existing as Cu CrO_2.

CONCLUSIONS

1. The Cu^+ species has been identified as the active site responsible for CO adsorption and subsequent CH_3OH formation in Cu–Cr oxide catalysts. This study represents the first time that direct experimental means (XPS, X-ray diffraction) have been used to identify the existence and role of Cu^+ in Cu-based, low-pressure CH_3OH synthesis catalysts.

2. The Cu^+ species is stable under reaction conditions and exists as a crystalline $CuCrO_2$ surface phase.

TABLE 4

Effect of High-Temperature Calcination on Catalytic and Physical Properties of Cu–Cr Oxide

Catalyst	Surface area (m^2/g)	Activity $\left(\frac{\mu\text{mole } CH_3OH}{\text{sec-m}^2 \text{ catalyst}}\right)$	$\frac{Cu^{+a}}{Cu_{tot}}$	Composition[b]
1/1 Cu/Cr (T_{calc} = 350°C, for 2 h)	21.4	0.02	0.21	$CuCrO_2$ (Minor)
1/1 Cu/Cr (T_{calc} = 1000°C, for 4 h)	2.9	0.06	0.5	$CuCrO_2$ (Major) $CuCr_2O_4$ (Major)

[a] Determined by XPS after H_2 reduction at 300°C.

[b] X-Ray diffraction data for calcined samples. After H_2 reduction, the $CuCr_2O_4$ peaks were replaced by Cu^0 peaks. The intensities of the $CuCrO_2$ peaks were not altered by H_2 reduction.

3. The concentration of surface Cu^+ (or $CuCrO_2$) is dependent upon:

(a) The Cu/Cr ratio. Catalytic activity and the amount of $CuCrO_2$ passes through a maximum at Cu/Cr ~0.7.

(b) The calcination temperature. For the normal Cu–Cr oxide catalyst prepared via the citrate route, a calcination temperature of ~350°C is optimal. X-Ray diffraction indicates that, below 350°C, there appears to be incomplete formation of $CuCrO_2$, and above 350°C, $CuCrO_2$ apparently decomposes. If high-temperature calcination (T = 1000°C) is used, however, $CuCrO_2$ becomes the thermodynamically stable phase, and enhancement of $CuCrO_2$ is observed.

ACKNOWLEDGMENTS

We gratefully acknowledge the assistance of E. Voll, C. Swanson, and T. Blanton for performing the surface area analyses, the neutron activation analyses, and the X-ray diffraction analyses, respectively.

REFERENCES

1. Monnier, J. R., Apai, G., and Hanrahan, M. J., *J. Catal.* **88,** 523 (1984).
2. Klier, K., "Advanced Methanol Synthesis Catalysts," 2nd Semiannual Technical Progress Report to ERDA and NSF (RANN), Grant AER-75-03776, December 10, 1976.
3. Herman, R. G., Klier, K., Simmons, G. W., Finn, B. P., Bulko, J. B., and Kobylinski, T. P., *J. Catal.* **56,** 407 (1979).
4. Herman, R. G., Klier, K., and Simmons, G. W., *in* "Proceedings, 7th International Congress on Catalysis, Tokyo, 1980" (T. Seiyama and K. Tanabe, Eds.), p. 475. Elsevier, Amsterdam, 1981.
5. Apai, G., Monnier, J. R., and Hanrahan, M. J., *J. Chem. Soc., Chem. Commun.*, 212 (1984).
6. Courty, P., Durand, D., Freund, E., and Sugier, A., *J. Mol. Catal.* **17,** 241 (1982).
7. Schreifels, J. A., Rodero, A., and Swartz, W. E., Jr., *Appl. Spectrosc.* **33,** 380 (1979).
8. Capece, F. M., DiCastro, V., Furlani, C., Mattogno, C., Fragale, C., Gargano, M., and Rossi, M., *J. Electron Spectrosc. Relat. Phenom.* **27,** 119 (1982).
9. Iimura, A., Inoue, Y., and Yasumuri, I., *Bull. Chem. Soc. Jpn.* **56,** 2203 (1983).
10. Burwell, R. L., Jr., Haller, G. L., Taylor, K. C., and Read, J. F., "Advances in Catalysis," Vol. 20, p. 1. Academic Press, New York, 1969.
11. Pasquali, M., Floriani, C., Gaetani-Manfredotti, A., and Guastini, C., *J. Amer. Chem. Soc.* **103,** 185 (1981).
12. Redhead, P. A., *Vacuum* **12,** 203 (1962).
13. Toyoshima, I., and Somorjai, G. A., *Catal. Rev.-Sci. Eng.* **19,** 105 (1979).
14. Stroupe, J. D., *J. Amer. Chem. Soc.* **71,** 569 (1949).